Structures and Buildings

ice Publishing

Cyclic response of masonry piers retrofitted with timber frames and boards

Gabriele Guerrini PE, PhD
Post-doctoral Researcher, Department of Civil Engineering and
Architecture (Dicar), University of Pavia, Pavia, Italy; European
Centre for Training and Research in Earthquake Engineering,
Eucentre, Pavia, Italy (Orcid:0000-0001-7853-3710)

Nicolò Damiani PE
PhD student, UME Graduate School, IUSS Pavia, Pavia, Italy
(Orcid:0000-0002-7221-963X)

Marco Miglietta PE
PhD student, UME Graduate School, IUSS Pavia, Pavia, Italy
(Orcid:0000-0002-0262-5106)

Francesco Graziotti PE, PhD
Assistant Professor, Department of Civil Engineering and Architecture
(Dicar), University of Pavia, Pavia, Italy; European Centre for Training
and Research in Earthquake Engineering, Eucentre, Pavia, Italy
(corresponding author: francesco.graziotti@unipv.it)
(Orcid:0000-0002-0223-0139)

The quasi-static in-plane cyclic response of two single-leaf calcium silicate unreinforced masonry piers was investigated
to show the effectiveness of an innovative timber retrofit solution. The aim of the intervention is to increase the pier
in-plane and out-of-plane strength and displacement capacity, thus reducing the seismic vulnerability of this typology
of unreinforced masonry construction with a light, cost-effective, sustainable and reversible approach. The retrofit
technique consists of a timber frame mechanically connected by means of steel fasteners to the masonry pier and
building floors. Oriented strand timber boards are then nailed to the frame. In-plane quasi-static shear–compression
cyclic tests were performed on two single-leaf calcium silicate brick piers with identical geometry and masonry
mechanical properties: one was tested unstrengthened while the other was tested in the retrofitted configuration. The
experimental results showed evident improvements in the lateral force–displacement response of the retrofitted
specimen. More specifically, compared with the bare masonry pier, the retrofitted pier exhibited slightly higher
stiffness, larger strength and significantly greater displacement capacity.

Notation

A_p	cross-sectional area of timber post
b_i	distance of the ith timber post in tension from the one in compression
$E_{0,mean}$	mean elastic modulus (parallel to fibres) of solid fir
E_m	masonry secant elastic modulus at 33% of its compressive strength
E_p	elastic modulus of timber post
F	horizontal shear force on pier
f_b	compressive strength of bricks
f_{bt}	tensile strength of bricks
f_c	compressive strength of mortar
$f_{c,0}$	characteristic compressive strength parallel to fibres of solid fir
f_m	compressive strength of masonry
f_t	tensile strength of mortar
$f_{t,0}$	characteristic tensile strength parallel to fibres of solid fir
f_{v0}	masonry shear strength at zero compression
f_w	masonry bond strength
G_m	masonry shear modulus ($G_m = 0.35E_m$)
H	height of pier
$K_{33\%}^{+}$	experimental secant stiffness at 33% of the maximum shear force in positive loading direction
K_{bl}^{+}	elastic stiffness in positive loading direction from bilinear idealisation
K_{mas}	analytical elastic stiffness of masonry pier
K_{OSB}	analytical shear stiffness of oriented strand board panels according to AWC (2008)
K_{tim}	analytical elastic stiffness of timber retrofit system
K_{tot}	analytical total elastic stiffness of retrofitted pier
L	length of pier
l_c	horizontal contact length at rocking interface
$M_{R,mas,f}$	analytical flexural strength of masonry pier due to flexural-rocking failure
$M_{R,tim,f}$	analytical flexural strength of timber retrofit system due to flexural failure
T_i	tensile axial force on i^{th} timber post
t	thickness of pier
u_{ix}	nodal displacement in x-direction for lateral displacement decomposition
u_{iy}	nodal displacement in y-direction for lateral displacement decomposition
V_{max}^{+}	experimental maximum shear force in positive loading direction
V_{max}^{-}	experimental maximum shear force in negative loading direction
$V_{R,fv0}$	analytical shear strength of masonry pier due to cohesion along horizontal joints
$V_{R,mas,f}$	analytical shear strength of masonry pier due to flexural-rocking failure
$V_{R,mas,s}$	analytical total shear strength of masonry pier due to sliding-shear failure
$V_{R,tim,f}$	analytical shear strength of timber retrofit system due to flexural failure

Structures and Buildings
Volume 174 Issue 5

**Cyclic response of masonry piers
retrofitted with timber frames and boards**
Guerrini, Damiani, Miglietta and Graziotti

$V_{R,tim,s}$	analytical shear strength of timber retrofit system due to shear failure
$V_{R,tot,f}$	analytical total shear strength of retrofitted pier due to flexural failure
$V_{R,tot,s}$	analytical total shear strength of retrofitted pier due to shear failure
$V_{R,\mu}$	analytical shear strength of masonry pier due to friction along horizontal joints
V_u^+	experimental shear force at ultimate displacement in positive loading direction
$V_{y,bl}^+$	yield strength in positive loading direction from bilinear idealisation
Z	sub-element height for lateral displacement decomposition ($= H/2$)
α_v	shear span ratio of pier
γ	shear deformation
δ	horizontal displacement of pier top
η	compressive stress-block magnitude of masonry
θ	pier drift ratio ($\theta = \delta/H$)
θ_{cr}^+	experimental first-crack drift ratio in positive loading direction
θ_{cr}^-	experimental first-crack drift ratio in negative loading direction
θ_u^+	experimental ultimate drift ratio in positive loading direction
θ_u^-	experimental ultimate drift ratio in negative loading direction
$\theta_{u,bl}^+$	ultimate drift ratio in positive loading direction from bilinear idealisation
θ_{Vmax}^+	experimental drift ratio at maximum recorded shear force in positive loading direction
θ_{Vmax}^-	experimental drift ratio at maximum recorded shear force in negative loading direction
θ_y	flexural deformation
$\theta_{y,bl}^+$	yield drift ratio in positive loading direction from bilinear idealisation
λ	compressive stress-block depth of masonry
μ	shear friction coefficient of masonry
ρ	density of masonry
σ_v	vertical compressive stress at mid-height of the masonry pier

1. Introduction

Unreinforced masonry cavity wall construction is a common solution for residential buildings in several parts of the world. When this construction typology is adopted in regions associated with low seismic hazard, it is often characterised by insufficient seismic details. However, recent events have demonstrated that both natural (i.e. the slip of an unknown fault (Horton and Williams, 2012)) and induced earthquakes (i.e. due to gas extraction (Bourne et al., 2015; Crowley et al., 2018; Graziotti et al., 2018)) can result in ground motions with intensity higher than anticipated in low-seismicity sites. These occurrences have prompted interest on possible retrofit

solutions to reduce the vulnerability of existing buildings in these regions.

Several retrofit techniques for unreinforced masonry have been investigated and implemented in the past. One of the most common interventions to improve the in-plane capacity of walls consists of applying an additional material layer to the masonry. These additional layers include fibre-reinforced composites (Alcaino and Santa-Maria, 2008; ElGawady et al., 2007; Luccioni and Rougier, 2011; Marcari et al., 2007; Mosallam and Banerjee, 2011; Tomaževič et al., 2015), fibre-reinforced cementitious matrices (Babaeidarabad et al., 2014; D'Ambrisi et al., 2013; Mantegazza et al., 2006) and externally bonded grids (Borri et al., 2011; Facconi et al., 2015; Giaretton et al., 2018; Papanicolaou et al., 2011; Prota et al., 2006; Yardim and Lalaj, 2016). Further possibilities for enhancement of the in-plane response include the application of steel elements mechanically connected to the masonry (Darbhanzi et al., 2014; Farooq et al., 2006; Taghdi et al., 2000) and the introduction of post-tensioning systems (Laursen and Ingham, 2001; Ma et al., 2012; Wight et al., 2006).

Similarly, the out-of-plane capacity of walls can be increased by applying fibre-reinforced strips or bars (Derakhshan et al., 2018; Galati et al., 2006; Willis et al., 2010), mortars reinforced with polymer textiles (Ismail and Ingham, 2016; Kadam et al., 2015; Kariou et al., 2018) or post-tensioning systems (Bailey et al., 2014; Ismail and Ingham, 2012; Popehn et al., 2007) to the masonry. Moreover, the improvement of connections between intersecting walls (Calderini et al., 2015; Calderini et al., 2019; Celik et al., 2009; Podestà and Scandolo, 2019) and between floor diaphragms and masonry walls (Moreira et al., 2014, 2016; Senaldi et al., 2019; Valluzzi, 2007) has proved to be effective in terms of both in-plane and out-of-plane behaviour enhancement.

Essential requirements for the suitability of retrofit systems for residential buildings in low-seismicity areas may include light weight, low cost, sustainability and reversibility. In light of these principles, retrofit systems made of timber are particularly interesting. With recognition of the ability of timber to supply tensile strength to masonry, combinations of masonry and timber as load-bearing structural systems have been adopted for buildings in seismic-prone zones for centuries (Cardoso et al., 2004; Gülkan and Langenbach, 2004; Tobriner, 1983). The seismic performance of existing masonry buildings that originally included timber elements for structural enhancement has been studied both numerically and experimentally (Graziotti et al., 2014; Kouris and Kappos, 2012; Meireles et al., 2012; Vintzileou, 2008). However, the application of timber as a retrofit solution to masonry elements has been proposed only recently. For example, Giaretton et al. (2016) and Dizhur et al. (2017) experimentally investigated the out-of-plane strengthening of slender masonry

Structures and Buildings
Volume 174 Issue 5

Cyclic response of masonry piers
retrofitted with timber frames and boards
Guerrini, Damiani, Miglietta and Graziotti

piers using timber strong-backs. Giongo *et al.* (2017) and Riccadonna *et al.* (2019) proposed and tested the use of cross-laminated timber panels connected to piers to enhance their in-plane capacity, while Sustersic and Dujic (2014) studied a similar technique for masonry infills.

Building on previous findings, the fundamental idea of the retrofit system discussed in this paper is to increase both the in-plane and out-of-plane capacities of masonry piers using a timber frame and oriented strand board (OSB) panels mechanically connected to the masonry, to the foundation and to the floor diaphragms. This paper presents and compares experimental results obtained from two in-plane quasi-static shear–compression cyclic tests on full-scale masonry piers with identical geometry and masonry mechanical properties – one consisting of bare masonry and the other strengthened using the proposed solution. The experimental campaign was conducted at the Eucentre laboratories in Pavia, Italy and at the Department of Civil Engineering and Architecture (DICAr) of the University of Pavia, Italy.

The geometry and loading conditions of the pier specimens reproduced the longest ground-floor pier of two Dutch terraced house full-scale prototypes. They were subjected to uni-directional dynamic shake-table tests (Damiani *et al.*, 2019; Miglietta *et al.*, 2018). These identical building prototypes were also tested in bare and retrofitted configurations, with the specific pier excited in-plane. All the processed data and instrumentation schemes of the quasi-static component tests and shake-table experiments are available elsewhere (Eucentre, 2020).

2. Description of test specimens

2.1 Masonry piers
The two single-wythe masonry piers consisted of 33 courses of calcium silicate bricks with average dimensions of $210 \times 100 \times 70$ mm and 10 mm thick mortar joints, resulting in height $H = 2{\cdot}70$ m, length $L = 2{\cdot}00$ m and thickness $t = 0{\cdot}10$ m (Figure 1). The two specimens were built simultaneously and aged under the same environmental conditions.

2.2 Retrofit system
The proposed masonry pier in-plane retrofit system consisted of a timber frame connected to the calcium silicate pier. It was conceived starting from the out-of-plane strengthening solution developed by Giaretton *et al.* (2016) and Dizhur *et al.* (2017), which relies on vertical timber strong-backs. The solution was further expanded to also increase the pier in-plane force and displacement capacity. The frame included vertical timber posts, coinciding with the strong-backs, and horizontal blocking (or nogging) elements. Timber sill plates allowed connection of the frame to the top reinforced concrete (RC) beam and to the footing. All the timber elements had a cross-section of 80×60 mm, where the smaller dimension was oriented perpendicular to the masonry walls. To increase the in-plane shear strength and stiffness of the specimen, 18 mm thick OSBs were fastened to the frame using 4 mm dia., 75 mm long anker nails at 100 mm spacing, following US design guidelines for timber shear walls (AWC, 2008; Figures 2 and 3). Member sizes were chosen to combine structural efficiency of the retrofit system with low invasiveness within real buildings.
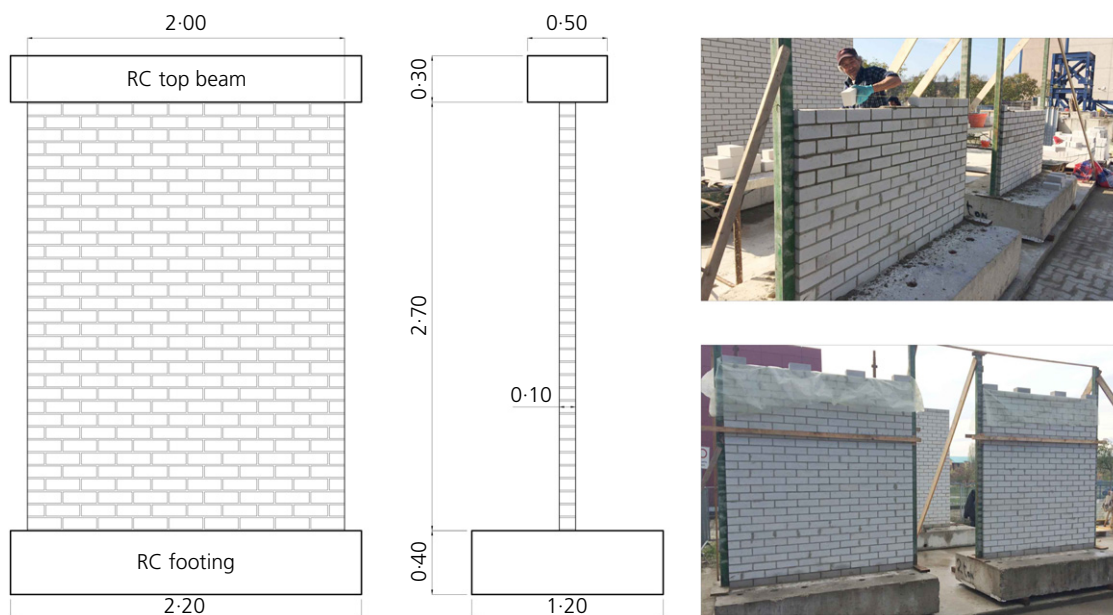

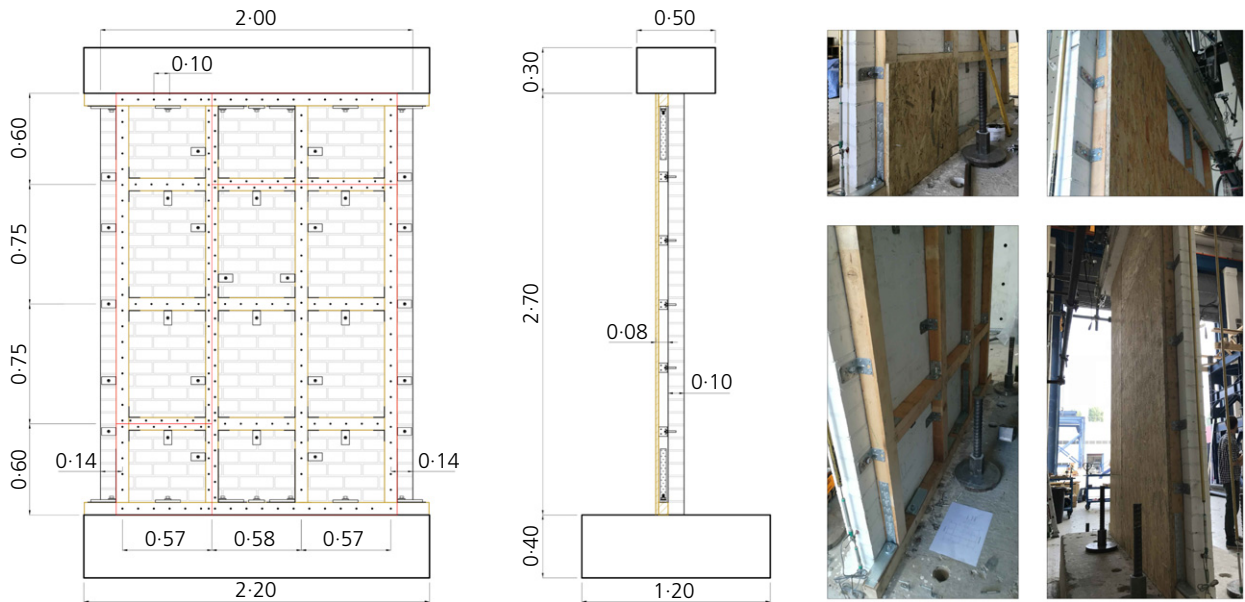**Figure 1.** Bare masonry pier geometry (dimensions in m)

Structures and Buildings
Volume 174 Issue 5

Cyclic response of masonry piers
retrofitted with timber frames and boards
Guerrini, Damiani, Miglietta and Graziotti

Figure 2. Retrofitted specimen geometry (dimensions in m)

Figure 3. Retrofit system components

Structures and Buildings
Volume 174 Issue 5

Cyclic response of masonry piers
retrofitted with timber frames and boards
Guerrini, Damiani, Miglietta and Graziotti
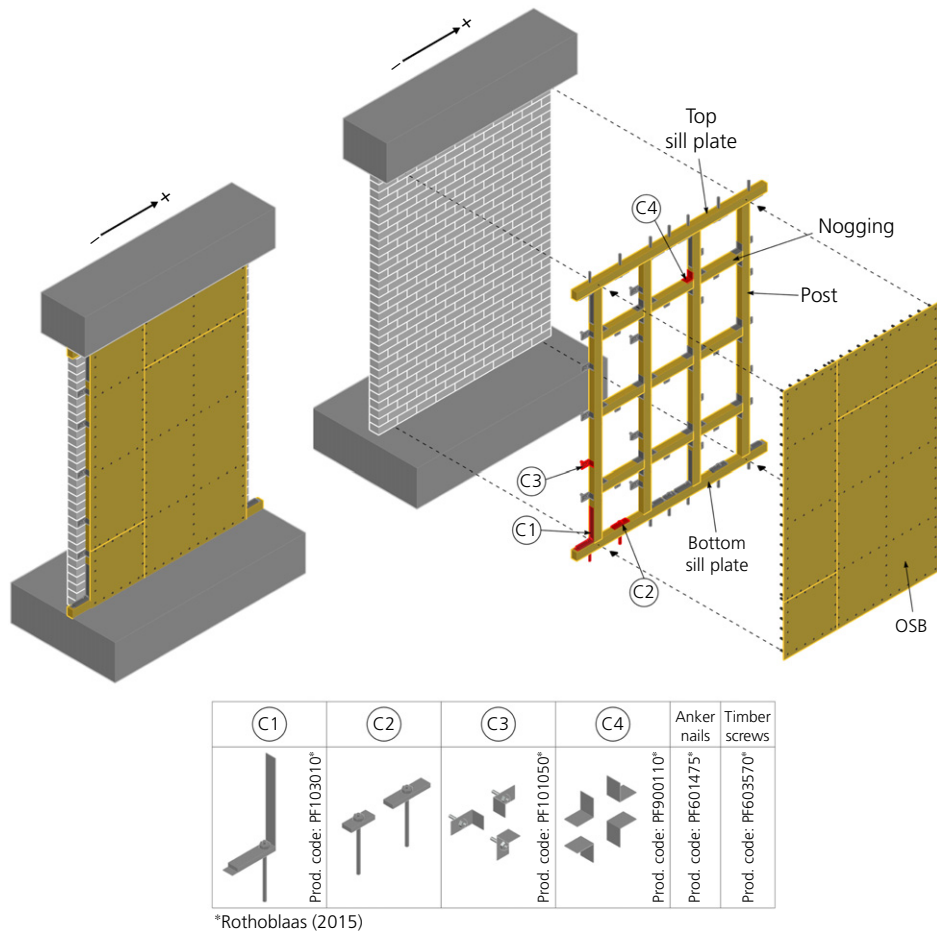
The effectiveness of the proposed solution depended on the connections between the timber elements, the masonry pier, the RC footing and the top beam. Four connection types (C1–C4) (Rothoblaas, 2015) were employed, as illustrated in Figure 3.

Connection type C1 indicates the tie-down anchorages that linked together the posts, top and bottom sill plates, and top and bottom RC elements. They were 340×182 mm steel angles with a cross-section of 40×2 mm fastened to the timber posts by 12 screws (5 mm dia., 70 mm long). The angles were connected to the RC elements through the sill plates by 12 mm dia. class 8·8 threaded rods bonded to the concrete with an epoxy adhesive, pre-tensioned at 33 kN, with $40 \times 160 \times 15$ mm rectangular steel anchor plates.
C2 are additional connections between the sill plates and RC elements through similar threaded rods and anchor plates, designed to prevent shear sliding.
C3 are the connections between the timber frame and masonry pier. 90×50 mm steel angles with a cross-section of 50×3 mm were connected to the timber members by four 5 mm dia., 70 mm long screws and to the masonry by a 10 mm dia. threaded rod bonded with an epoxy adhesive.
C4 indicates the connections between posts and blocking elements provided by 70×70 mm steel angles with a cross-section of 55×2 mm, connected to the timber members by five 5 mm dia., 70 mm long screws on each leg. Four angles were provided at intersections with interior posts, while only two were provided at intersections with edge posts.

The cost of the materials employed to strengthen the specimen was approximately €130 per square metre of wall surface (market prices in Northern Italy). The required installation time was estimated to be 2·5 man-hours per square metre of wall surface, considering its application to an entire full-scale building prototype (Damiani *et al.*, 2019).

2.3   Mechanical properties of materials

2.3.1   Calcium silicate masonry
All mechanical characterisation tests on the masonry were performed at the DICAr laboratory of the University of Pavia in 2018 on specimens that were 28 d old. A detailed overview of the characterisation campaign can be found elsewhere (Miglietta *et al.*, 2018).

The main material properties are summarised in Table 1. Calcium silicate bricks were tested in compression and bending according to BS EN 772-1:2011 (BSI, 2011) to obtain their compressive strength (f_b) and tensile strength (f_{bt}). The tensile (f_t) and compressive (f_c) strengths of the mortar were determined according to the prescriptions of BS EN 1015-11:2019 (BSI, 2006a); sand was added to the mix to reproduce the properties measured in situ on existing buildings more closely. The compressive strength of the masonry (f_m) and the secant elastic modulus at 33% of compressive strength (E_m) were obtained by testing masonry wallettes in compression along the direction perpendicular to the horizontal bed-joints, according to BS EN 1052-1:1999 (BSI, 1998). The initial shear strength (f_{v0}) and the friction coefficient (μ) were obtained according to BS EN 1052-3:2002 (BSI, 2002), while the masonry bond strength (f_w) was obtained following BS EN 1052-5:2005 (BSI, 2005a). The masonry density (ρ) was 1837 kg/m^3.

2.3.2   Retrofit components
Red solid fir (*Picea abies*), with a density of 517 kg/m^3 and belonging to category S10/C24 according to BS EN 14081-1:2016 (BSI, 2016), was used to construct the timber frames. Its characteristic compressive strength parallel to the fibres ($f_{c,0}$) was 21 MPa, its characteristic tensile strength parallel to the fibres ($f_{t,0}$) was 14 MPa and its mean Young modulus ($E_{0,mean}$) was 11000 MPa. The OSB boards had a density of 572 kg/m^3 and belonged to category OSB/3 according to BS EN 300:2006 (BSI, 2006b). Only the densities were determined at the DICAr laboratory; all the other properties were taken as specified by the mentioned codes.

The steel angles used for tie-down connections C1 had a characteristic tensile strength of 11·6 kN, while those for the frame-to-masonry connections C3 had a characteristic shear strength of 3·3 kN (Rothoblaas, 2015).

The epoxy adhesive offered characteristic tensile and shear strengths of 41 kN and 20 kN respectively when applied to 10 mm dia. rods. These strengths increased to 59 kN and 30 kN respectively when used with 12 mm dia. rods. These values refer to embedment in uncracked concrete (Hilti, 2019).

3.   Testing procedure

3.1   Test setup
The experimental setup used for the in-plane shear–compression cyclic tests on both specimens is shown in Figure 4. The RC footing was bolted to the laboratory strong

Table 1. Mechanical properties of masonry

	Bricks		Mortar		Masonry					
	f_b	f_{bt}	f_c	f_t	f_m	E_m	f_w	f_{v0}	μ	ρ
Number of tested specimens	6	12	63	63	6	6	30	14	14	6
Average	19·8 MPa	2·5 MPa	5·06 MPa	1·74 MPa	10·1 MPa	6593 MPa	0·28 MPa	0·62 MPa	0·71	1837 kg/m^3
Coefficient of variation	0·18	0·09	0·24	0·28	0·06	0·09	0·32	—	—	0·01

Structures and Buildings
Volume 174 Issue 5

**Cyclic response of masonry piers
retrofitted with timber frames and boards**
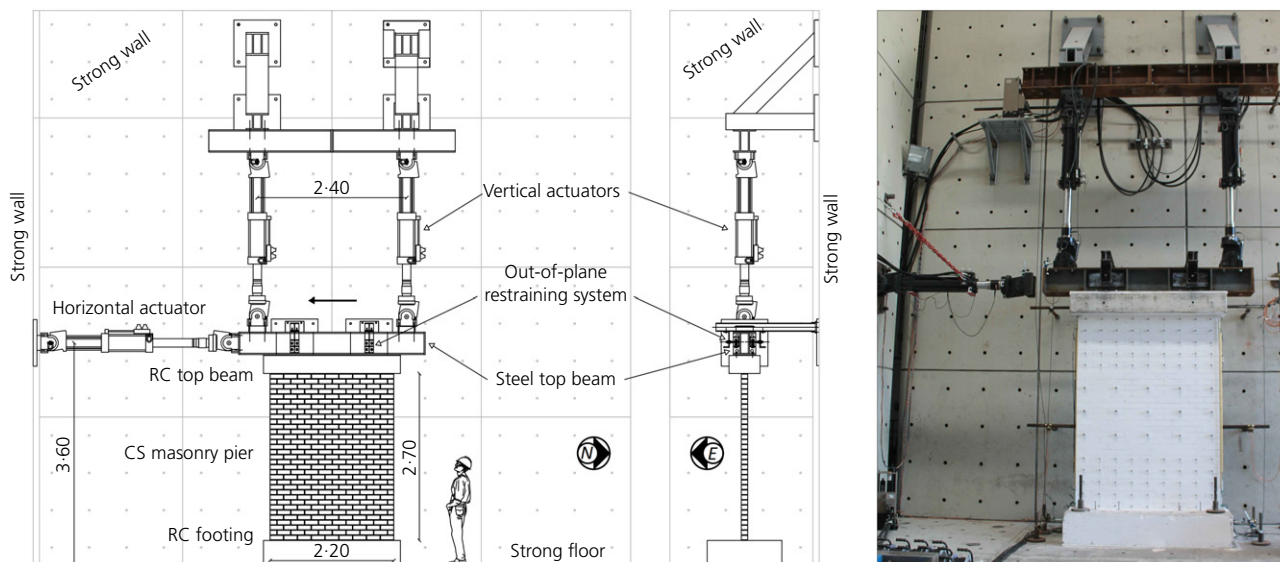Guerrini, Damiani, Miglietta and Graziotti

Figure 4. In-plane shear–compression cyclic tests setup (dimensions in m)

floor. A steel beam was fastened to the top RC beam. To achieve continuous and uniform contact, a layer of self-levelling high-strength shrinkage-controlled gypsum was placed between the RC footing and the strong floor and between the RC top beam and the steel beam.

Two vertical servo-hydraulic actuators, reacting against a steel frame fixed to the laboratory strong wall, were connected to the steel top beam, providing double-curvature boundary conditions. A horizontal servo-hydraulic actuator reacted against the strong wall and pushed/pulled the specimen through the top steel beam. A restraining system connecting the top steel beam to the strong wall limited the RC top beam rotations about its longitudinal axis and the out-of-plane displacements of the pier, forcing an in-plane response up to severe damage conditions.

3.2 Instrumentation and data acquisition
The forces applied by the three actuators were continuously monitored by load cells. Horizontal, vertical and diagonal displacements were recorded by transducers mounted at several locations throughout the specimen, allowing the determination of significant deformation parameters.

In addition to load cells and potentiometers, an optical acquisition system with high-resolution cameras was used to monitor the three-dimensional trajectories of passive reflective markers, distributed over one surface of the specimens (the grey dots visible in the photo in Figure 4).

3.3 Loading protocol
Both specimens were subjected to the same vertical overburden stress of 0·5 MPa at the top and were tested under double-curvature, consistent with the boundary conditions of masonry

piers located in the first storey of a typical Dutch two-storey terraced house (Miglietta *et al.*, 2018). The applied overburden stress represented an upper-bound scenario and was evaluated considering the increase in axial load due to rocking and uplift of the pier corners.

In the first step, the vertical actuators applied axial load with a constant loading rate. In the case of the retrofitted pier, a gap of 10 mm was left between the vertical posts and the top sill plate while the top row of nails had not yet been provided to the OSB during this loading phase. This allowed the vertical load to be carried by the masonry pier without significant participation of the frame, as would happen in real situations. Fastening operations were then completed after full application of the axial force.

The horizontal loading history followed a force-controlled procedure for the firsts two sets of cycles, after which loading was continued in displacement-controlled mode. Each set included three push–pull cycles of equal amplitude; the duration of the cycles was kept almost constant, varying the displacement rate proportionally to the target displacement. The target forces (F), displacements (δ) and drift ratios ($\theta = \delta/H$) of each cycle set for both specimens are provided in Table 2. The positive loading direction was associated with the actuator pulling the specimen southward and the negative direction was associated with pushing northward.

4. Experimental results

4.1 Unstrengthened specimen
The bare specimen initially exhibited a rocking behaviour. The first horizontal crack was observed at the bottom of the pier (Figure 5(a)) at drift ratios $\theta_{cr}^+ = \theta_{cr}^- = \pm0·075\%$ in both the

Structures and Buildings
Volume 174 Issue 5

Cyclic response of masonry piers
retrofitted with timber frames and boards
Guerrini, Damiani, Miglietta and Graziotti

positive and negative directions, along the first and second bed-joints above the base of the wall. The damage pattern at the end of the cycles when the maximum positive shear was achieved (i.e. $\theta_{V\mathrm{max}}^+ = 0.20\%$) is shown in Figure 5(b).

At a drift ratio of 0·25%, the top horizontal flexural crack extended throughout the whole length of the specimen, between the 32nd and 33rd brick courses above the base, allowing the onset of sliding at the top of the wall. The specimen began to behave asymmetrically in positive and negative directions during the cycles at a drift ratio of 0·40%: the wall kept sliding along the top crack when the actuator was pushing, while it rocked when the actuator was pulling.

Table 2. Nominal lateral loading protocol

Cycle set	F: kN	δ: mm	θ: %	Velocity: mm/s
Unstrengthened and retrofitted piers				
1	15	—	—	—
2	25	—	—	—
3	—	0·50	0·02	0·01
4	—	0·90	0·03	0·02
5	—	1·30	0·05	0·03
6	—	2·00	0·075	0·04
7	—	2·70	0·10	0·05
8	—	4·00	0·15	0·08
9	—	5·40	0·20	0·10
10	—	6·70	0·25	0·15
11	—	8·10	0·30	0·15
12	—	10·80	0·40	0·20
13	—	13·50	0·50	0·30
Retrofitted pier				
14	—	16·20	0·60	0·40
15	—	21·50	0·80	0·50
16	—	26·90	1·00	0·60
17	—	40·40	1·50	1·00
18	—	53·90	2·00	1·50

During the cycles at a drift ratio of 0·50%, despite the presence of rotational restraints, the top beam started rotating about its longitudinal axis, inducing out-of-plane displacements on the pier, probably due to extensive toe crushing at the base of the specimen and high out-of-plane slenderness. The test continued with a monotonic lateral loading procedure and was terminated when the specimen lost its vertical load-bearing capacity. The pier failed at an ultimate drift $\theta_u^+ = 0.75\%$ in the positive loading direction (Figure 5(c)).

The recorded hysteretic loops are shown in Figure 6. The overall response of the specimen was characterised by rocking behaviour up to a drift ratio of 0·20%. The maximum negative shear, $V_{\mathrm{max}}^- = 74.5$ kN, was reached at $\theta_{V\mathrm{max}}^- = 0.15\%$, while the maximum positive shear, $V_{\mathrm{max}}^+ = 77.9$ kN, was reached at $\theta_{V\mathrm{max}}^+ = 0.20\%$. After reaching the maximum positive resistance, the development of a continuous top horizontal crack at the pier top changed the behaviour to a shear-sliding mechanism. In fact, the hysteretic cycles became significantly wider, denoting greater energy dissipation due to friction between the brick courses sliding across the continuous crack. The asymmetrical behaviour observed during the test starting at a drift ratio of 0·40% was confirmed by the shape of the hysteretic cycles: wider, sliding-dominated cycles were obtained in the negative direction, as opposed to narrower, re-centring, rocking-dominated cycles in the positive direction.

The total lateral displacement was decomposed into the contributions of flexural deformation (θ_y) and shear deformation (γ), following the procedure developed by Seible and Igarashi (1991) as depicted in Figure 7. Because the test was performed under double-curvature conditions, the contributions were computed assuming the inflection point at mid-height of the specimen and analysing the top and bottom halves of the pier separately; accordingly, each half was characterised by height
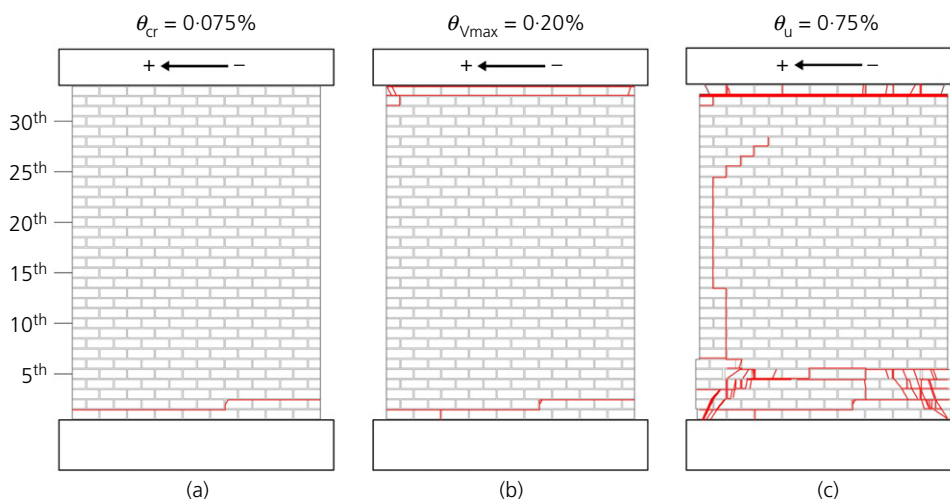

Figure 5. Bare pier crack pattern corresponding to: (a) first cracking; (b) maximum recorded shear; (c) ultimate conditions
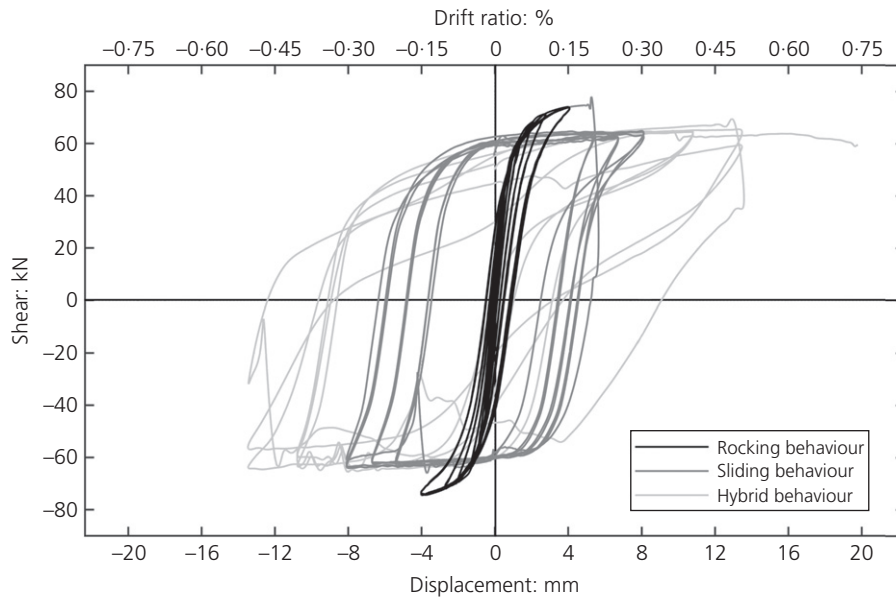
Structures and Buildings
Volume 174 Issue 5

**Cyclic response of masonry piers
retrofitted with timber frames and boards**
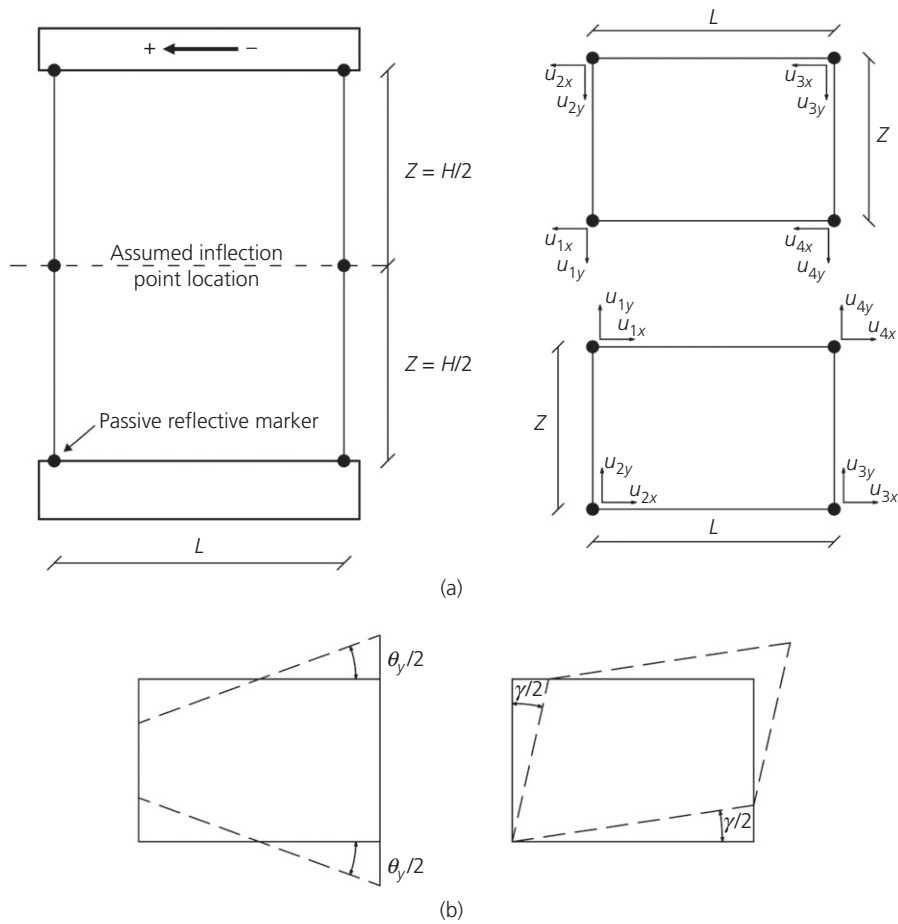Guerrini, Damiani, Miglietta and Graziotti

Figure 6. Bare pier hysteretic response

Figure 7. Displacement contributions: (a) sub-elements with reference nodes; (b) flexural and shear deformation modes

Structures and Buildings
Volume 174 Issue 5

**Cyclic response of masonry piers
retrofitted with timber frames and boards**
Guerrini, Damiani, Miglietta and Graziotti

$Z = H/2$. The displacements of six points (Figure 7), obtained from the trajectories of the passive reflective markers, were used to calculate the displacement components: two at the edges of the RC footing, two at the specimen mid-height and two at the edges of the RC top beam.

Figure 8 shows the percentage of the lateral displacement contributed by flexural and shear deformations recorded at maximum positive and negative displacements during the first cycle of each set of three. Some minor discrepancies were observed between the sum of the two contributions and the total displacement (labelled 'other' in Figure 8); this was likely due to instrumentation tolerances and inflection point deviations from the mid-height. The two components were comparable up to a drift ratio of 0·15%. After that, the flexural effect dropped significantly while the shear component, which

included sliding over the horizontal crack at the top of the specimen, became dominant.

4.2 Retrofitted specimen

The first two cracks developed above the second brick layer (Figure 9(a)) at drift ratios $\theta_{cr}^+ = \theta_{cr}^- = 0.075\%$ in both positive and negative directions, as was observed for the bare pier. A crack pattern characteristic of a toe crushing mechanism started to develop at the bottom corners of the specimen after reaching a drift ratio of 0·15% and became evident after reaching 0·20% (Figure 9(b)). During these loading stages, two horizontal cracks also extended continuously throughout the pier length: one above the second brick course and one above the fifth course, at the level of the lowermost timber post-to-masonry connections. It should be noted that, at 0·20% drift ratio, the bare pier exhibited its maximum shear strength with the onset of a sliding mechanism. The cycles at drift ratios of 0·25% and 0·30% were characterised by toe crushing propagation at both bottom corners, which also caused the expulsion of portions of bricks and mortar.

The first damage to a retrofit component was observed at a drift ratio of 0·60%: the steel angles of the tie-down connections (C1 in Figure 3) at the top corners of the specimen buckled in compression. Figure 9(c) shows the damage pattern after the specimen reached its maximum shear strength at drift ratios $\theta_{Vmax}^+ = \theta_{Vmax}^- = \pm0.80\%$, which also corresponded to the ultimate drift ratio of the unstrengthened pier: extensive toe crushing was visible, with dislocation and loss of significant portions of masonry at the lower corners. The following cycles at a drift ratio of 1·00% resulted in buckling of the tie-down steel angles at the base of the specimen.

During the pulling phase at a drift ratio of 1·50%, a diagonal shear crack with a slope of about 45° formed in the top half of the specimen. This was probably caused by the shear deformation reached by the pier, which could not be accommodated
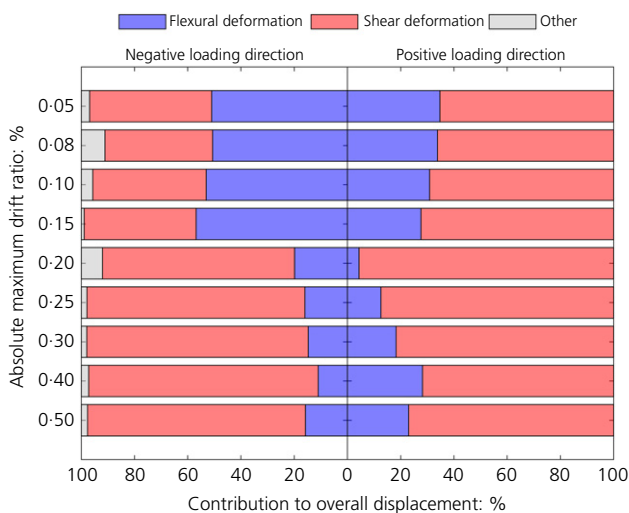

Figure 8. Bare pier displacement contributions. A full-colour version of this figure can be found on the ICE Virtual Library (www.icevirtuallibrary.com)
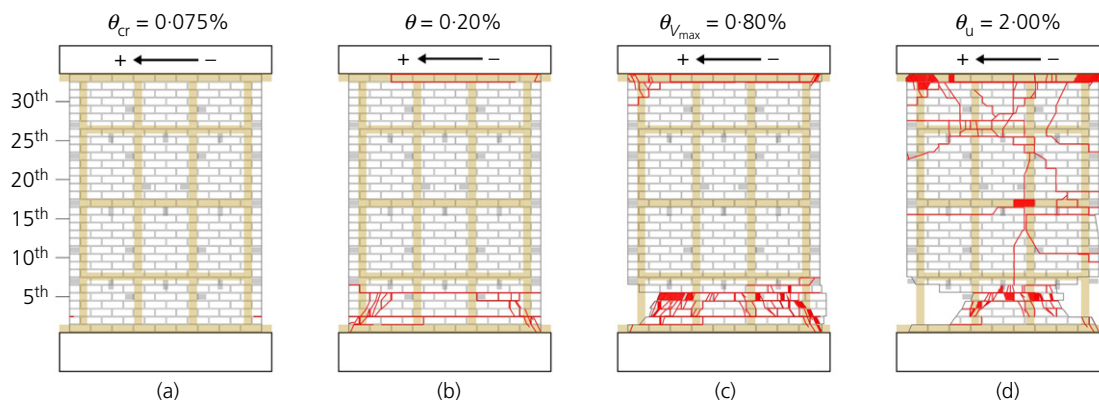

Figure 9. Retrofitted pier crack pattern corresponding to: (a) first cracking; (b) maximum recorded shear on the bare pier; (c) ultimate conditions of the bare pier and maximum recorded shear on the retrofitted pier; (d) ultimate conditions

Structures and Buildings
Volume 174 Issue 5

Cyclic response of masonry piers
retrofitted with timber frames and boards
Guerrini, Damiani, Miglietta and Graziotti

by the masonry. The last cycles performed at $\theta_u^+ = \theta_u^- = \pm 2 \cdot 00\%$ caused extensive damage to the specimen. During the pushing and pulling phases, new diagonal, vertical and horizontal cracks developed throughout the wall (Figure 9(d)). The tie-down steel angles were visibly buckled, while the axial compression transferred by the posts resulted in dents in the top and bottom sill plates, with a depth of a few millimetres.

The test was stopped after completing two cycles at a drift ratio of $\pm 2 \cdot 00\%$. At this stage the masonry pier was no longer able to withstand the vertical load, which was likely almost entirely carried by the timber posts. The transfer of axial force from the masonry to the timber system was inferred by correlating the progressive lowering of the pier top with the cycle maximum drift ratios. As shown in Figure 10, the downward (negative) displacements became significant after overcoming the experimental ultimate drift ratio of the bare pier, reaching 22 mm at the end of the test.

The experimental hysteretic loops of the retrofitted pier are shown in Figure 11. The specimen reached its maximum positive and negative shear strength ($V_{max}^+ = 104 \cdot 7$ kN and $V_{max}^- = -109 \cdot 6$ kN) at drift ratios $\theta_{Vmax}^+ = \theta_{Vmax}^- = \pm 0 \cdot 80\%$ (Figure 9(c)). After these points, a progressive strength degradation was recorded when pulling; the strength remained almost constant under pushing until it suddenly dropped during the second-last set of cycles upon diagonal shear cracking of the masonry.

The total displacement was decomposed into the contributions of flexural deformation (θ_y) and shear deformation (γ), as was done for the bare pier. Figure 12 shows their percentages recorded at maximum positive and negative displacements during the first cycle of each set of three. The proportions remained similar throughout the entire test without sudden changes, except for a slight reduction in the flexural contributions during the cycles at drift ratios of 0·20% and 0·25%. This may be associated with the formation of two continuous

cracks in the lower portion of the pier, with possible onset of a sliding mechanism (as observed for the bare pier) partially inhibited by the stiffness of the timber retrofit.

Figure 13 shows the axial deformation of the bottom-north tie-down connection and the shear deformation of a portion of OSB sheathing against the horizontal displacement. The tie-down connections showed a stable tension–compression response up to a drift ratio of 0·80%; then, progressive shortening was observed, related to the extensive buckling of the steel angles and the denting of the sill plates (Figure 13(a)). It is interesting to note that the shortening of the top and bottom tie-down connections, the denting of the sill plates and the compressive axial deformation of the posts resulted in an overall shortening of the timber system compatible with the top beam
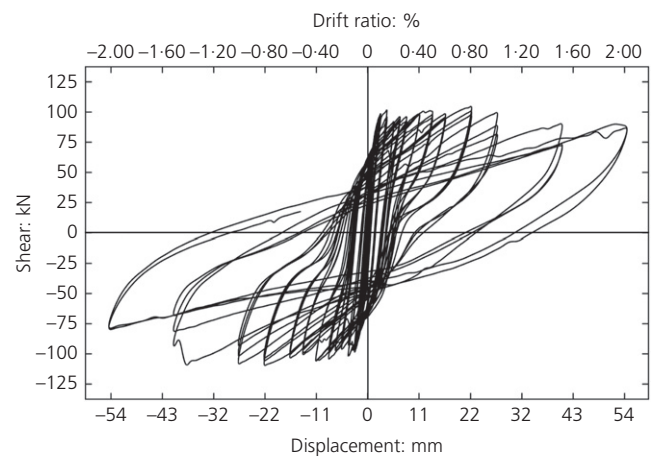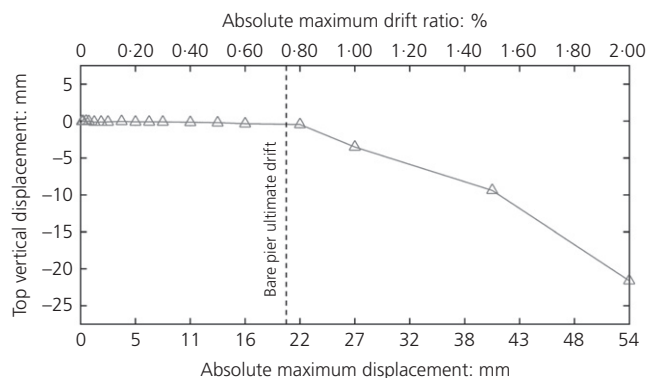

Figure 11. Retrofitted pier hysteretic response
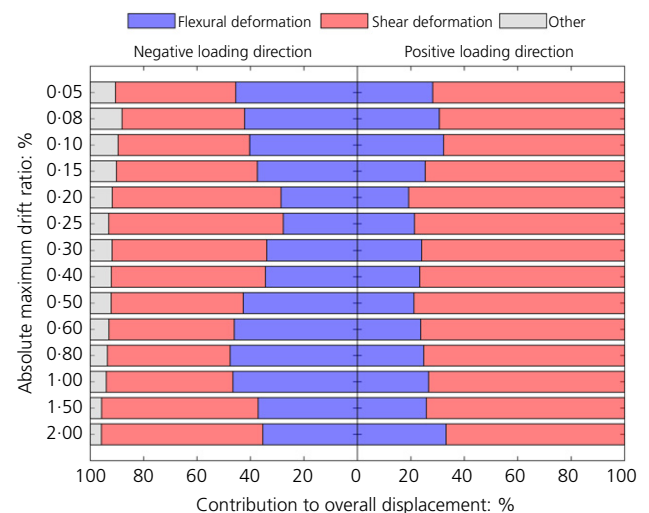

Figure 12. Retrofitted pier displacement contributions. A full-colour version of this figure can be found on the ICE Virtual Library (www.icevirtuallibrary.com)

Figure 10. Retrofitted pier: vertical displacement of the pier top at zero lateral force

Structures and Buildings
Volume 174 Issue 5

**Cyclic response of masonry piers
retrofitted with timber frames and boards**
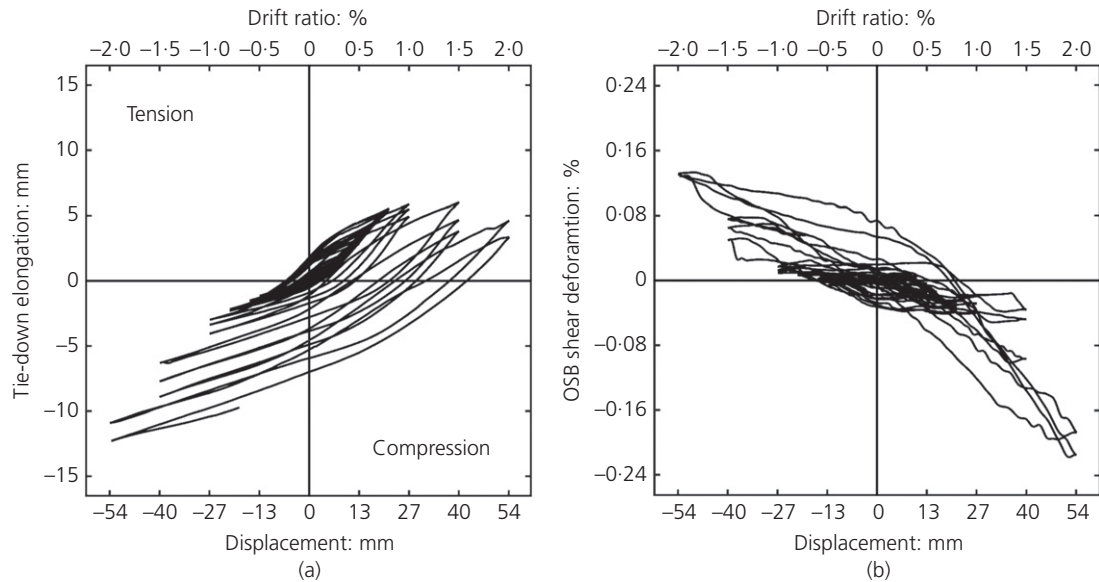Guerrini, Damiani, Miglietta and Graziotti

Figure 13. Retrofit system response: (a) elongation of the tie-down connection at the bottom-north corner; (b) OSB shear deformation

22 mm downward displacement shown in Figure 10. The shear deformation of the OSB became significant at a drift ratio of 1·50%, after reaching a value of 0·05% (Figure 13(b)): this corresponded to diagonal shear cracking of the masonry and was consistent with the cracking shear deformation obtained for calcium silicate squat piers by Graziotti *et al.* (2016).

4.3 Comparison of test results

The experimental backbone curves of both piers in the positive loading direction and their bilinear idealisations are compared in Figure 14. The backbone curves include the maximum-force points for all cycles and the maximum-displacement point for the last cycle. Table 3 provides a summary of the main experimental results for the positive loading direction in terms of the secant stiffness at 33% of the maximum shear force ($K^+_{33\%}$), the first-cracking drift ratio (θ^+_{cr}), the maximum drift ratio ($\theta^+_{V\max}$) and the corresponding shear force ($V^+_{\max}$) and the ultimate drift ratio (θ^+_u) and corresponding shear force (V^+_u).

The idealised bilinear relationships were defined following the work of Morandi *et al.* (2018). The elastic stiffness (K^+_{bl}) was taken as the slope of the secant line through the experimental point at 70% of the maximum shear ($V^+_{\max}$), while the ultimate drift ratio ($\theta^+_{u,bl}$) was set at a strength drop equal to 20% of $V^+_{\max}$. The yield point ($\theta^+_{y,bl}$, $V^+_{y,bl}$) was obtained by intersecting the secant line with a horizontal one and imposing the equivalence of the areas below the experimental envelope and the idealised bilinear curve up to $\theta^+_{u,bl}$. The parameters defining the bilinear relationships are summarised in Table 4.

It is interesting to note that the retrofit system, characterised by a stiffness equal to about 10% of that of the masonry pier,
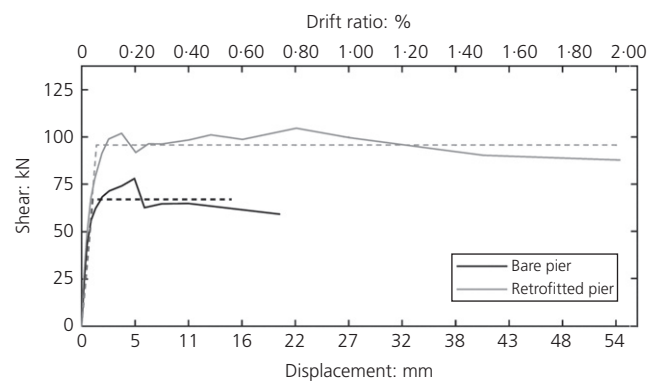

Figure 14. Backbone curves and bilinear idealisations of the bare and retrofitted piers (positive loading direction)

began working after the first cracking of the masonry, which occurred at a drift ratio of 0·075% (Figure 14). For smaller displacements, the initial stiffnesses of the two specimens were nearly identical, as typically observed in reinforced masonry and RC elements. Both specimens exhibited a sudden drop of strength at drift ratios of 0·20%, when horizontal cracks extended continuously throughout the pier length (Figure 15). However, while the bare pier did not recover this loss because of the transition from a rocking to a sliding behaviour, the stiffness of the timber retrofit inhibited shear sliding along the cracks and allowed the specimen to reach higher displacements, gaining additional strength.

Figures 16(a) and 16(b) show the ultimate state of the bare pier and the retrofitted pier, respectively. Both specimens presented significant toe crushing, which was more pronounced

Structures and Buildings
Volume 174 Issue 5

Cyclic response of masonry piers
retrofitted with timber frames and boards
Guerrini, Damiani, Miglietta and Graziotti

Table 3. Backbone curve parameters, positive loading direction

	$K_{33\%}^+$: kN/mm	θ_{cr}^+: %	θ_{Vmax}^+: %	V_{max}^+: kN	θ_u^+: %	V_u^+: kN
Bare pier	94	0·075	0·2	78	0·75	59
Retrofitted pier	106	0·075	0·8	105	2·00	88

Table 4. Bilinear idealisation parameters, positive loading direction

	K_{bl}^+: kN/mm	$\theta_{y,bl}^+$: %	$V_{y,bl}^+$: kN	$\theta_{u,bl}^+$: %
Bare pier	60·9	0·04	67·0	0·56
Retrofitted pier	64·3	0·06	95·7	2·00

on the retrofitted wall. In fact, the bare pier failed due to out-of-plane distortion induced by deterioration at the rocking/sliding interfaces, which limited its in-plane drift capacity. The retrofitted specimen sustained more than twice the lateral displacement as the timber system allowed exploitation of the full flexural-rocking capacity and gradually took over the masonry compression resistance.

At the end of the test, although the masonry was heavily damaged, the timber frame helped the retrofitted pier maintain gravity load resistance, while the bare pier lost its vertical load-bearing capacity. Damage to the retrofit was localised within the tie-down connections, with the steel angles yielded in tension and buckled in compression (Figure 16(c)), and within the top and bottom sill plates, where the posts transferred concentrated compressive forces.

The cumulative dissipated energy for the two piers is shown in Figure 17. Although the piers were characterised by different failure mechanisms and hysteretic loop shapes, the dissipated energy was similar up to failure of the bare pier. Indeed, the latter exhibited wider cycles with lower strength, governed by the shear-sliding mechanism, while the retrofitted pier showed slightly thinner cycles with higher strength.

The dissipated energy was converted into equivalent viscous damping, according to Jacobsen (1960). These results are plotted in Figure 18 against the maximum drift ratio of each cycle. For each drift ratio increment, the average area enclosed by the three cycles was first computed and then converted into an equivalent viscous damping ratio. The bare pier offered higher equivalent viscous damping after the transition from rocking to shear-sliding behaviour at a drift ratio of 0·20% because a sliding-governed response results in wider hysteretic loops. On the other hand, the flexure-controlled retrofitted pier exhibited smaller equivalent viscous damping, which slightly decreased as damage progressed at larger drift ratios.

5. Analytical prediction of experimental results

In this section, simple equations are proposed to capture the elastic stiffness and the strength of the retrofitted pier, which can be used for the design of the retrofit system. The analytical results were validated against the experimental results obtained in the positive loading direction as summarised in Table 3.
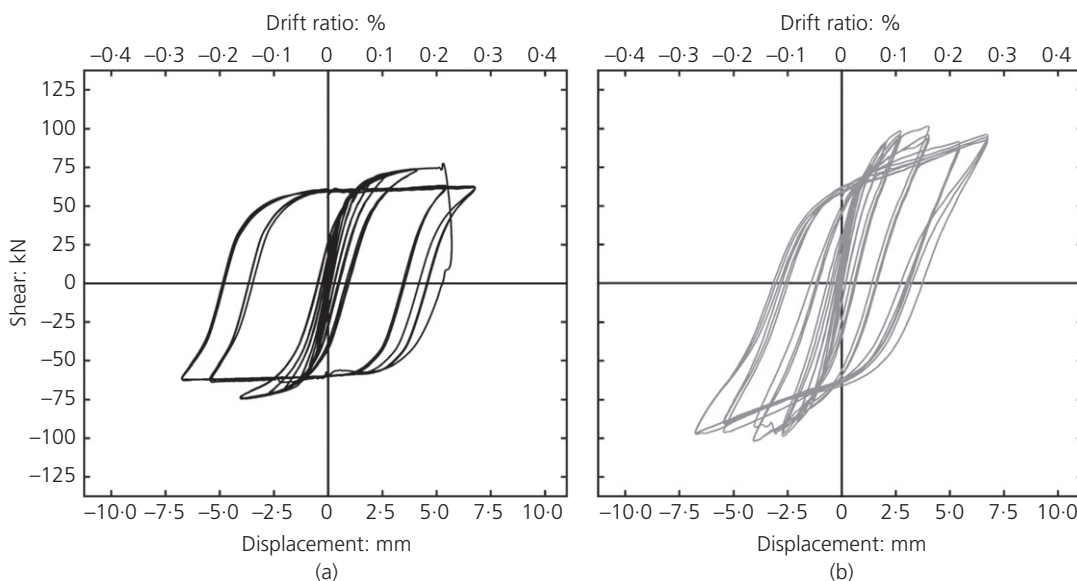

Figure 15. Hysteretic response up to 0·25% drift ratio: (a) bare pier; (b) retrofitted pier

Structures and Buildings
Volume 174 Issue 5

Cyclic response of masonry piers
retrofitted with timber frames and boards
Guerrini, Damiani, Miglietta and Graziotti

(a)　　　　　　(b)　　　　　　(c)

Figure 16. Ultimate conditions: (a) bare pier; (b) retrofitted pier; (c) buckled tie-down steel angle
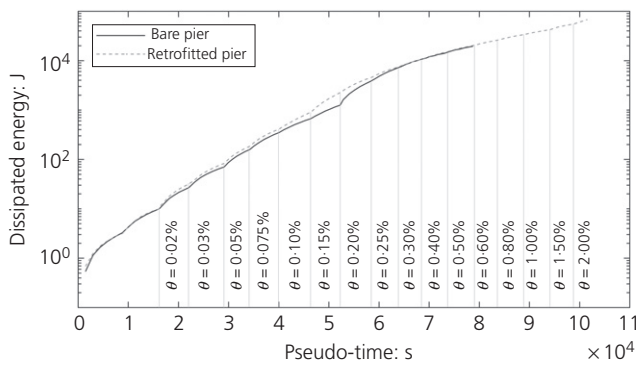

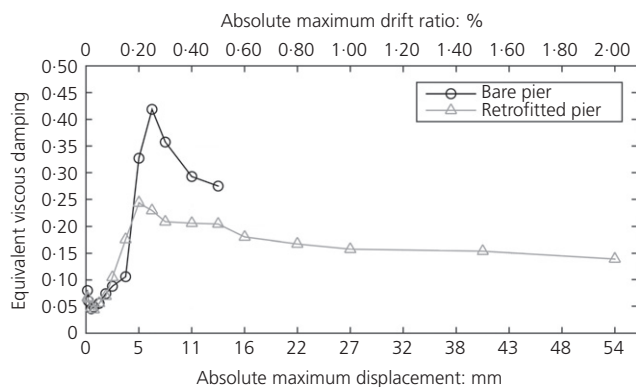**Figure 17.** Bare and retrofitted pier hysteretic energy dissipation

Figure 18. Bare and retrofitted pier equivalent viscous damping

5.1 Unstrengthened specimen

For double-curvature boundary conditions the masonry wall initial stiffness can be calculated as

1.
$$K_{mas} = \left(\frac{H^3}{E_m L^3 t} + 1 \cdot 2 \frac{H}{G_m L t} \right)^{-1}$$

where E_m is the masonry modulus of elasticity, G_m is the shear modulus (assumed equal to $0 \cdot 35 E_m$ according to MIT (2018)) and H, L and t are the height, length and thickness of the pier, respectively.

Substituting the dimensions and material properties of the bare pier into Equation 1 yields $K_{mas} = 95$ kN/mm. Thus, compared with the experimental secant stiffness at 33% of the maximum shear force (94 kN/mm), Equation 1 results in a negligible overestimation of the order of 1%.

The lateral strength associated with a flexural-rocking mechanism can be obtained from Equation 2 (Magenes and Calvi, 1997)

2.
$$V_{R,mas,f} = \frac{2 M_{R,mas,f}}{H}$$

with the bending moment resistance ($M_{R,mas,f}$) of the end sections evaluated as

3.
$$M_{R,mas,f} = \frac{\sigma_v L^2 t}{2} \left(1 - \frac{\sigma_v}{\eta f_m} \right)$$

Structures and Buildings
Volume 174 Issue 5

**Cyclic response of masonry piers
retrofitted with timber frames and boards**
Guerrini, Damiani, Miglietta and Graziotti

where σ_v is the vertical compressive stress evaluated on the gross masonry section at the mid-height of the pier, t is the wall thickness and η is the stress-block magnitude parameter, which is assumed to be equal to 0·85. For the tested pier, the vertical compressive stress of 0·524 MPa at mid-height results in an rocking shear strength $V_{R,mas,f} = 74$ kN.

The estimated sliding-shear strength of the specimen due to frictional ($V_{R,\mu}$) and cohesive ($V_{R,fv0}$) contributions can be calculated as (BSI, 2005b; Magenes and Calvi, 1997)

$$4. \qquad V_{R,mas,s} = V_{R,\mu} + V_{R,f_{v0}} = \mu\sigma_v tL + f_{v0}tl_c$$

with the contact length (l_c) given by

$$5. \qquad L\left(\frac{\sigma_v}{\eta\lambda f_m}\right) \leq \left[l_c = 1\cdot5L\left(1 - \alpha_v\frac{3f_{v0} + 2\mu\sigma_v}{\sigma_v + 3f_{v0}\alpha_v}\right)\right] \leq L$$

where μ is the friction coefficient, σ_v is the vertical compressive stress, f_{v0} is the masonry initial shear strength, f_m is the masonry compressive strength and α_v ($= H/(2L) = 0\cdot67$) is the shear span ratio. The stress-block depth parameter λ, generally ranging from 0·7 to 1·0, can be taken equal to 0·85. The estimated sliding-shear strength of the specimen is then $V_{R,mas,s} = 84$ kN.

With the sliding-shear strength being slightly higher than the rocking lateral strength, the development of a flexural mechanism would be expected before the onset of sliding. In fact, the minimum computed strength $V_{R,mas,f} = 74$ kN provides a good estimation of the actual experimental strength of 78 kN, with an error of about 5%.

Moreover, the same equations can be used to estimate the residual shear strength after the sliding mechanism activation at 0·2% drift ratio, which resulted in a hybrid response of the specimen. This transition was caused by the opening of a full-length flexural crack at the top of the specimen, resulting in loss of cohesion and an experimental residual strength of about 65 kN. Evaluating the frictional shear resistance only, $V_{R,\mu} = 75$ kN, results in a 15% overestimation of this residual sliding-shear strength.

5.2 Retrofitted specimen

The lateral stiffness and strength of the retrofitted pier can be calculated under the simplifying assumption that masonry and timber act as springs in parallel, thus their individual contributions can be directly summed. Accordingly, the elastic stiffness of the timber retrofit system can be computed using Equation 6 (Countryman, 1952)

$$6. \qquad K_{tim} = \left(\frac{H^3}{6E_pA_pL^2} + \frac{H}{K_{OSB}L}\right)^{-1}$$

where E_p is the elastic modulus of the timber post, A_p is the cross-sectional area of each outermost post and K_{OSB} is the shear stiffness of the nailed OSB panels. For the case under examination, $E_p = E_{0,mean} = 11\,000$ MPa and a nominal cross-section area of $A_p = 4800$ mm^2 were adopted for the timber, while a nominal shear stiffness $K_{OSB} = 15\,500$ N/mm was assigned to the OSB according to the US specification for timber shear walls (AWC, 2008). The in-plane elastic stiffness of the timber retrofit system then becomes $K_{tim} = 9\cdot8$ kN/mm. The experimental counterpart of 12 kN/mm can be obtained from Table 3 by subtracting the stiffness of the bare pier (94 kN/mm) from the that of the retrofitted specimen (106 kN/mm). This results in an underestimation of the retrofit stiffness of 18%. However, the timber retrofit accounts for only about 10% of the total lateral stiffness. Comparing the total predicted stiffness $K_{tot} = K_{mas} + K_{tim} = 105$ kN/mm with the experimental stiffness of the retrofitted pier (106 kN/mm), the error is only 1%.

The flexural-rocking strength of the retrofit system is provided by the vertical forces acting on the timber posts. All the posts are assumed to be stressed by the same tensile force, except for an outermost post that carries compression. Rotational equilibrium can be written with respect to the compression post, since no axial load is assumed to be carried by the timber

$$7. \qquad M_{R,tim,f} = \sum(T_i b_i)$$

where T_i is the tensile axial force in the ith post and b_i its distance from the compression post. The tensile forces are the minimum between the tensile strength of the timber post and the yield strength of the vertical leg of the steel angle in connection C1 in Figure 3. The lateral strength associated with flexural failure can then be calculated using Equation 8.

$$8. \qquad V_{R,tim,f} = \frac{2M_{R,tim,f}}{H}$$

For the tested pier, the tensile strength of the posts was $1\cdot5A_pf_{t,0} = 100\cdot5$ kN, while the mean yield capacity of the connection was $1\cdot1 \times 11\cdot6$ kN $= 12\cdot8$ kN and controlled the force on the posts. This results in $V_{R,tim,f} = 33$ kN. The factors 1·5 and 1·1 account for mean-to-nominal (or mean-to-characteristic) strength ratio according to ASCE (2017).

The strength associated with a shear failure mode of the retrofit system is mainly provided by the OSB nailed to the timber frame. The shear strength can be predicted in accordance with the US specifications for timber shear walls (ASCE, 2017; AWC, 2008), where it is a function of the nominal panel thickness, the fastener penetration into the framing members and the panel edge fastener spacing. A shear strength $V_{R,tim,s} = 45$ kN can be derived for the specific case. However,

Structures and Buildings
Volume 174 Issue 5

Cyclic response of masonry piers
retrofitted with timber frames and boards
Guerrini, Damiani, Miglietta and Graziotti

considering that such values are derived for shear walls without blocking elements and nailed only along the panel edges, a slightly higher shear strength may be expected when intermediate nailing is also provided.

The retrofitted pier strength depends on the mechanism that will develop, controlled by either flexure or shear. The strength of the bare pier and of the retrofit system associated with the corresponding failure mode need to be summed together, and the smaller value indicates the correct mechanism. For the specific case, $V_{R,tot,f} = V_{R,mas,f} + V_{R,tim,f} = 107$ kN and $V_{R,tot,s} = V_{R,mas,s} + V_{R,tim,s} = 129$ kN: this indicates a flexural failure mode, as observed experimentally, with an error of less than 2% on the actual strength of 105 kN (Table 3). The predicted strength of the retrofit system ($V_{R,tim,f} = 33$ kN) is affected by a 22% error compared with the experimental value of 27 kN obtained from Table 3 as the difference between the retrofitted and bare pier strength.

6. Conclusions

A timber retrofit solution applied to a single-leaf unreinforced masonry pier built with calcium silicate bricks to enhance its in-plane seismic resistance was investigated. The proposed retrofit system consisted of a timber frame mechanically connected to the masonry pier, to the foundation and to the top beam, and OSB panels nailed to the frame.

Two specimens with the same masonry dimensions and material properties – one a bare masonry pier and the other completed with the retrofit – were subjected to cyclic in-plane shear–compression tests under the same level of axial compression and boundary conditions. All the processed data and instrumentation schemes can be obtained elsewhere (Eucentre, 2020).

The unstrengthened specimen showed hybrid behaviour, developing first a flexural-rocking mechanism that then evolved into a sliding-shear mode. The first cracks appeared at a drift ratio of 0·075%, while ultimate conditions were reached at a drift ratio of 0·75% with out-of-plane distortion of the severely damaged specimen. The maximum recorded lateral strength was approximately 78 kN.

The retrofitted pier maintained flexural behaviour up to 1·50% drift ratio because the timber frame inhibited shear-sliding and allowed some flexural overstrength to develop. The first cracks appeared at a drift ratio of 0·075%, as in the bare pier, while an ultimate drift ratio of 2·00% was reached when diagonal shear cracks were formed within the masonry. Extensive toe crushing affected the base corners of the retrofitted masonry pier, with almost all the vertical load carried by the timber frame at ultimate conditions. The only damage to the retrofit system was localised within the tie-down connection steel angles, which yielded and buckled, and within the timber sill plates, which were dented upon compression transfer from the posts. The maximum shear attained was about 105 kN.

Significant improvements of the seismic performance were achieved. Even though the timber retrofit did not delay first cracking, due to its high flexibility compared with the masonry pier, it allowed an increase in the specimen's ultimate displacement (by 167%) and its lateral strength (by 35%). The effectiveness of the proposed retrofit system depended on the good connection quality and on the top beam and foundation resistance to the transferred stresses.

Analytical predictions of the in-plane stiffness and strength of the two specimens resulted in good agreement with the experimental values, with errors always within 5%. These formulae will serve for the future development of design guidelines.

For practical applications, because the proposed retrofit system stems from previous studies where the timber posts acted as strong-backs for out-of-plane response, it can not only enhance the in-plane behaviour of piers but can also improve their out-of-plane resistance. To demonstrate its global effectiveness, the system was applied to a full-scale building prototype tested on the shake-table of the Eucentre laboratories in Pavia, Italy.

Acknowledgements

REFERENCES

Alcaino P and Santa-Maria H (2008) Experimental response of externally retrofitted masonry walls subjected to shear loading. *Journal of Composites for Construction* **12(5)**: 489–498.

ASCE (American Society of Civil Engineers) (2017) ASCE/SEI 41-17: Seismic evaluation and retrofit of existing buildings. ASCE, Reston, VA, USA.

AWC (American Wood Council) (2008) ANSI/AF&PA SDPWS-2008: Special design provisions for wind and seismic. AWC, Washington, DC, USA.

Babaeidarabad S, Arboleda D, Loreto G and Nanni A (2014) Shear strengthening of un-reinforced concrete masonry walls with fabric-reinforced-cementitious-matrix. *Construction and Building Materials* **65**: 243–253.

Bailey S, Dizhur D, Trowsdale and Griffith M (2014) Performance of posttensioned seismic retrofit of two stone masonry buildings during the Canterbury earthquakes. *Journal of Performance of Constructed Facilities* **29(4)**: 04014111.

Structures and Buildings
Volume 174 Issue 5

Cyclic response of masonry piers
retrofitted with timber frames and boards
Guerrini, Damiani, Miglietta and Graziotti

Borri A, Castori G and Corradi M (2011) Shear behavior of masonry panels strengthened by high strength steel cords. *Construction and Building Materials* **25(2)**: 494–503.

Bourne SJ, Oates SJ, Bommer JJ et al. (2015) A Monte Carlo method for probabilistic hazard assessment of induced seismicity due to conventional natural gas production. *Bulletin of the Seismological Society of America* **105(3)**: 1721–1738.

BSI (1998) BS EN 1052-1:1999: Methods of test for masonry. Determination of compressive strength. BSI, London, UK.

BSI (2002) BS EN 1052-3:2002: Methods of test for masonry units. Determination of initial shear strength. BSI, London, UK.

BSI (2005a) BS EN 1052-5:2005: Methods of test for masonry. Determination of bond strength by the bond wrench method. BSI, London, UK.

BSI (2005b) BS EN 1996: Eurocode 6: Design of masonry structures. Part 1-1: General rules for buildings. Rules for reinforced and unreinforced masonry. BSI, London, UK.

BSI (2006a) BS EN 1015-11:2019: Methods of test for mortar for masonry. Determination of flexural and compressive strength of hardened mortar. BSI, London, UK.

BSI (2006b) BS EN 300:2006: Oriented strand board (OSB). Definitions, classification and specifications. BSI, London, UK.

BSI (2011) BS EN 772-1:2011: Methods of test for masonry units. Determination of compressive strength. BSI, London, UK.

BSI (2016) BS EN 14081-1:2016: Timber structures. Strength graded structural timber with rectangular cross section. General requirements. BSI, London, UK.

Calderini C, Lagomarsino S and Rossi M (2015) Shaking table tests of an arch-pillars system and design of strengthening by the use of tie-rods. *Bulletin of Earthquake Engineering* **13(1)**: 279–297.

Calderini C, Piccardo P and Vecchiattini R (2019) Experimental characterization of ancient metal tie-rods in historic masonry buildings. *International Journal of Architectural Heritage* **13(3)**: 425–437.

Cardoso R, Lopes M and Bento R (2004) Earthquake resistant structures of Portuguese old 'pombalino' buildings. *Proceedings of the 13th WCEE, Vancouver, BC, Canada*, Paper No. 918.

Celik O, Sesigur H and Cili F (2009) Importance of wood and iron tension members on seismic performance of historic masonry buildings: three case studies from Turkey. *Paper presented at the ATC and SEI Conference on Improving the Seismic Performance of Existing Buildings and Other Structures, San Francisco, CA, USA*, pp. 1374–1383.

Countryman D (1952) *Lateral Tests on Plywood Sheathed Diaphragms: Laboratory Report No. 55*. Douglas Fir Plywood Association, Tacoma, WA, USA.

Crowley H, Pinho R, van Elk J and Uilenreef J (2018) Probabilistic damage assessment of buildings due to induced seismicity. *Bulletin of Earthquake Engineering* **17(8)**: 4495–4516.

D'Ambrisi A, Mezzi M and Caporale A (2013) Experimental investigation on polymeric net-RCM reinforced masonry panels. *Composite Structures* **105**: 207–215.

Damiani N, Miglietta M, Mazzella L et al. (2019) *Full-scale Shaking Table Test on A Dutch URM Cavity-Wall Terraced-House end Unit – A Retrofit Solution with Strong-Backs and OSB Boards – EUC-BUILD-7*. Eucentre foundation, Pavia, Italy, Research report EUC052/2019U.

Darbhanzi A, Marefat MS and Khanmohammadi M (2014) Investigation of in-plane seismic retrofit of unreinforced masonry walls by means of vertical steel ties. *Construction and Building Materials* **52**: 122–129.

Derakhshan H, Lucas W, Visintin P and Griffith MC (2018) Laboratory testing of strengthened cavity unreinforced masonry walls. *Journal of Structural Engineering* **144(3)**: 04018005.

Dizhur D, Giaretton M, Giongo I and Ingham JM (2017) Seismic retrofit of masonry walls using timber strong-backs. *SESOC Journal* **30(2)**: 1–30.

ElGawady MA, Lestuzzi P and Badoux M (2007) Static cyclic response of masonry walls retrofitted with fiber-reinforced polymers. *Journal of Composites for Construction* **11(1)**: 50–61.

Eucentre (2020) See http://www.eucentre.it/nam-project (accessed 25/02/2020).

Facconi L, Conforti A, Minelli F and Plizzari GA (2015) Improving shear strength of unreinforced masonry walls by nano-reinforced fibrous mortar coating. *Materials and Structures* **48(8)**: 2557–2574.

Farooq SH, Ilyas M and Ghaffar A (2006) Technique for strengthening of masonry wall panels using steel strips. *Asian Journal of Civil Engineering (Building and Housing)* **7(6)**: 621–638.

Galati N, Tumialan G and Nanni A (2006) Strengthening with FRP bars of URM walls subject to out-of-plane loads. *Construction and Building Materials* **20(1–2)**: 101–110.

Giaretton M, Dizhur D and Ingham JM (2016) Shaking table testing of as-built and retrofitted clay brick URM cavity-walls. *Engineering Structures* **125**: 70–79.

Giaretton M, Dizhur D, Garbin E, Ingham J and da Porto F (2018) In-plane strengthening of clay brick and block masonry walls using textile-reinforced mortar. *Journal of Composites for Construction* **22(5)**: 04018028.

Giongo I, Schiro G and Piazza M (2017) On the use of timber-based panels for the seismic retrofit of masonry structures. *Proceedings of Prohitech 3rd International Conference on Protection of Historical Constructions, Lisbon, Portugal*.

Graziotti F, Penna A and Magenes G (2014) Influence of timber lintels on the cyclic behaviour of stone masonry spandrels. *Proceedings of International Masonry Conference 2014, Guimarães, Portugal*.

Graziotti F, Rossi A, Mandirola M, Penna A and Magenes G (2016) Experimental characterisation of calcium-silicate brick masonry for seismic assessment. *Brick and Block Masonry: Trends, Innovations and Challenges – Proceedings of the 16th International Brick and Block Masonry Conference, IBMAC, Padua, Italy*, pp. 1619–1628.

Graziotti F, Penna A and Magenes G (2018) A comprehensive in situ and laboratory testing programme supporting seismic risk analysis of URM buildings subjected to induced earthquakes. *Bulletin of Earthquake Engineering* **17(8)**: 4575–4599.

Gülkan P and Langenbach R (2004) The earthquake resistance of traditional timber and masonry dwellings in Turkey. *Proceedings of 13th WCEE, Vancouver, BC, Canada*, Paper No. 2297.

Hilti (2019) *Hilti Technical Datasheet: HIT-RE 500 V3 Injection Mortar*. Hilti, Schaan, Liechtenstein.

Horton Jr JW and Williams RA (2012) The 2011 Virginia earthquake: What are scientists learning? *Eos* **93(33)**: 317–318.

Ismail N and Ingham JM (2012) Cyclic out-of-plane behavior of slender clay brick masonry walls seismically strengthened using posttensioning. *Journal of Structural Engineering* **138(10)**: 1255–1266.

Ismail N and Ingham JM (2016) In-plane and out-of-plane testing of unreinforced masonry walls strengthened using polymer textile reinforced mortar. *Engineering Structures* **118**: 167–177.

Jacobsen LS (1960) Damping in composite structures. *Proceedings of the 2nd World Conference on Earthquake Engineering, Tokyo and Kyoto, Japan*. vol. 2, pp. 1029–1044.

Kadam SB, Singh Y and Li B (2015) Out-of-plane behaviour of unreinforced masonry strengthened using ferrocement overlay. *Materials and Structures* **48(10)**: 3187–3203.

Kariou FA, Triantafyllou SP, Bournas DA and Koutas JN (2018) Out-of-plane response of masonry walls strengthened using

Structures and Buildings
Volume 174 Issue 5

Cyclic response of masonry piers
retrofitted with timber frames and boards
Guerrini, Damiani, Miglietta and Graziotti

textile-mortar system. *Construction and Building Materials* **165**:
769–781.

Kouris LAS and Kappos AJ (2012) Detailed and simplified non-linear
models for timber-framed masonry structures. *Journal of Cultural
Heritage* **13(1)**: 47–58.

Laursen PT and Ingham JM (2001) Structural testing of single-storey
post-tensioned concrete masonry walls. *The Masonry Society
Journal* **19(1)**: 69–82.

Luccioni B and Rougier VC (2011) In-plane retrofitting of masonry
panels with fibre reinforced composite materials. *Construction and
Building Materials* **25(4)**: 1772–1788.

Ma R, Jiang L, He M, Fang C and Liang F (2012) Experimental
investigations on masonry structures using external prestressing
techniques for improving seismic performance. *Engineering
Structures* **42**: 297–307.

Magenes G and Calvi GM (1997) In-plane seismic response of brick
masonry walls. *Earthquake Engineering & Structural Dynamics*
26(11): 1091–1112.

Mantegazza G, Gatti A and Barbieri A (2006) Retrofitting
concrete and masonry building: FRCM (fiber reinforced
cementitious matrix) a new emerging technology.
*Proceedings of XII Konferencja Naukowo-Techniczna Problemy
Remontowe W Budownictwie Ogólnym I Obiektach Zabytkowych*,
pp. 6–8.

Marcari G, Manfredi G, Prota A and Pecce M (2007) In-plane shear
performance of masonry panels strengthened with FRP.
Composites Part B: Engineering **38(7–8)**: 887–901.

Meireles H, Bento R, Cattari S and Lagomarsino S (2012) A hysteretic
model for 'frontal' walls in pombalino buildings. *Bulletin of
Earthquake Engineering* **10(5)**: 1481–1502.

Miglietta M, Mazzella L, Grottoli L, Guerrini G and Graziotti F (2018)
*Full-scale Shaking Table Test on A Dutch URM Cavity-Wall
Terraced-House End Unit – EUC-BUILD-6.* Eucentre Foundation,
Pavia, Italy, Research Report EUC160/2018U.

MIT (Ministero Infrastrutture e Trasporti) (2018) *Norme Tecniche per le
Costruzioni.* MIT, Rome, Italy (in Italian).

Morandi P, Albanesi L, Graziotti F *et al.* (2018) Development of a
dataset on the in-plane experimental response of URM piers
with bricks and blocks. *Construction and Building Materials* **190**:
593–611.

Moreira S, Ramos LF, Oliveira DV and Lourenco PB (2014) Experimental
behavior of masonry wall-to-timber elements connections
strengthened with injection anchors. *Engineering Structures* **81**:
98–109.

Moreira S, Ramos LF, Oliveira DV and Lourenco PB (2016) Design
parameters for seismically retrofitted masonry-to-timber
connections: injection anchors. *International Journal of
Architectural Heritage* **10(2–3)**: 217–234.

Mosallam A and Banerjee S (2011) Enhancement in in-plane shear
capacity of unreinforced masonry (URM) walls strengthened with
fiber reinforced polymer composites. *Composites Part B:
Engineering* **42(6)**: 1657–1670.

Papanicolaou C, Triantafillou T and Lekka M (2011) Externally bonded
grids as strengthening and seismic retrofitting materials of
masonry panels. *Construction and Building Materials* **25(2)**:
504–514.

Podestà S and Scandolo L (2019) Earthquakes and tie-rods: assessment,
design, and ductility issues. *International Journal of Architectural
Heritage* **13(3)**: 329–339.

Popehn JRB, Schultz AE and Drake CR (2007) Behavior of slender,
posttensioned masonry walls under transverse loading. *Journal of
Structural Engineering* **133(11)**: 1541–1550.

Prota A, Marcari G, Fabbrocino G, Manfredi G and Aldea C (2006)
Experimental in-plane behavior of tuff masonry strengthened with
cementitious matrix–grid composites. *Journal of Composites for
Construction* **10(3)**: 223–233.

Riccadonna D, Giongo I, Schiro G, Rizzi E and Parisi MA (2019)
Experimental shear testing of timber-masonry dry connections for
the seismic retrofit of unreinforced masonry shear walls.
Construction and Building Materials **211**: 52–72.

Rothoblaas (2015) See http://www.rothoblaas.com/catalogues-
rothoblaas (accessed 25/02/2020).

Seible F and Igarashi A (1991) Full scale testing of masonry structures
under simulated seismic loadings. In *Experimental and Numerical
Methods in Earthquake Engineering* (Donea J and Jones PM
(eds)). Kluwer Academic Publishing, Dordrecht, the Netherlands,
pp. 119–148.

Senaldi I, Guerrini G, Caruso M *et al.* (2019) Experimental seismic
response of a half-scale stone masonry building aggregate: effects
of retrofit strategies. In *Structural Analysis of Historical
Constructions* (Aguilar R, Torrealva D, Moreira S, Pando MA and
Ramos LF (eds)). Springer, Cham, Switzerland, pp. 1372–1381.

Sustersic I and Dujic B (2014) Seismic shaking table testing of a
reinforced concrete frame with masonry infill strengthened with
cross laminated timber panels. *Proceedings of World Conference on
Timber Engineering, WCTE 2014, Quebec City, Canada.*

Taghdi M, Bruneau M and Saatcioglu M (2000) Seismic retrofitting of
low-rise masonry and concrete walls using steel strips. *Journal of
Structural Engineering* **126(9)**: 1017–1025.

Tobriner S (1983) La casa baraccata: earthquake-resistant construction
in 18th-century Calabria. *Journal of the Society of Architectural
Historians* **42(2)**: 131–138.

Tomaževič M, Gams M and Berset T (2015) Strengthening of stone
masonry walls with composite reinforced coatings. *Bulletin of
Earthquake Engineering* **13(7)**: 2003–2027.

Valluzzi MR (2007) On the vulnerability of historical masonry
structures: analysis and mitigation. *Materials and Structures* **40(7)**:
723–743.

Vintzileou E (2008) Effect of timber ties on the behavior of historic
masonry. *Journal of Structural Engineering* **134(6)**: 961–972.

Wight GD, Ingham JM and Kowalsky MJ (2006) Shaketable testing of
rectangular post-tensioned concrete masonry walls. *ACI Structural
Journal* **103(4)**: 587.

Willis CR, Seracino R and Griffith MC (2010) Out-of-plane strength of
brick masonry retrofitted with horizontal NSM CFRP strips.
Engineering Structures **32(2)**: 547–555.

Yardim Y and Lalaj O (2016) Shear strengthening of unreinforced
masonry wall with different fiber reinforced mortar jacketing.
Construction and Building Materials **102**(Part 1): 149–154.

How can you contribute?

To discuss this paper, please email up to 500 words to the
editor at journals@ice.org.uk. Your contribution will be
forwarded to the author(s) for a reply and, if considered
appropriate by the editorial board, it will be published as
discussion in a future issue of the journal.

Proceedings journals rely entirely on contributions from the
civil engineering profession (and allied disciplines).
Information about how to submit your paper online
is available at www.icevirtuallibrary.com/page/authors,
where you will also find detailed author guidelines.